arXiv:2206.11563v1 [cs.LG] 23 Jun 2022

LED: Latent Variable-based Estimation of Density

Omri Ben-Dov *
omri.ben-dov@tuebingen.mpg.de

Pravir Singh Gupta
Mythic Inc.
pravir.singh.gupta@gmail.com

Victoria Fernandez Abrevaya*
victoria.abrevaya@tuebingen.mpg.de

Michael J. Black*
black@tuebingen.mpg.de

Partha Ghosh*
partha.ghosh@tuebingen.mpg.de

Abstract

Modern generative models are roughly divided into two main categories: (1) models that can produce high-quality random samples, but cannot estimate the exact density of new data points and (2) those that provide exact density estimation, at the expense of sample quality and compactness of the latent space. In this work we propose LED, a new generative model closely related to GANs, that allows not only efficient sampling but also efficient density estimation. By maximizing log-likelihood on the output of the discriminator, we arrive at an alternative adversarial optimization objective that encourages generated data diversity. This formulation provides insights into the relationships between several popular generative models. Additionally, we construct a flow-based generator that can compute exact probabilities for generated samples, while allowing low-dimensional latent variables as input. Our experimental results, on various datasets, show that our density estimator produces accurate estimates, while retaining good quality in the generated samples.

1 Introduction

Generative models strive to extract some notion of the data distribution given a set of training data, either explicitly through a probability density (e.g., Van den Oord et al. (2016b)), indirectly through a stochastic sampling mechanism (e.g., Goodfellow et al. (2014)), or both (e.g., Dinh et al. (2014)). The current state of the art for generative modeling – GANs Goodfellow et al. (2014) – can handle large-dimensional data such as images with impressive performance, but they have only an *implicit* notion of the distribution: they can generate random samples, but cannot compute the likelihood of a new data point. Access to an explicit density function, however, provides several advantages: quantitative comparison among models becomes straightforward; training through maximum likelihood estimation (MLE) has been proven to be asymptotically statistically efficient Huber (1967); and applications such as unsupervised or semi-supervised learning can benefit from this prior knowledge.

Autoregressive models Van den Oord et al. (2016a,b) and normalizing flows Dinh et al. (2014) are among the most prominent examples of deep generative models that compute exact probability and employ direct log-likelihood maximization of their training dataset. However, it is inefficient to sample from autoregressive models, and they do not provide a latent representation of the data.

*Max Planck Insitute of Intelligent Systems

Preprint. Under review.

Normalizing flows, on the other hand, allow both efficient sampling and density estimation, but make restrictive assumptions on the model architecture, requiring the latent space to be of the same dimensionality as the input, making it computationally expensive to use them in the high-dimensional data regime.

Energy-Based models (EBMs)Song and Kingma (2021) and Variational Autoencoders (VAEs) Kingma and Welling (2014) are also deep generative models based on likelihood maximization. However, VAEs can only compute a lower bound of the likelihood and imposes restrictive assumptions on the family of distributions it can represent, resulting in inter-sample averaging. Consequently, when applied to images, VAEs generate blurry samples. EBMs, on the other hand, represent an unnormalized density, allowing greater flexibility in the choice of the functional form, at the cost of inefficient sampling and likelihood estimation.

In this work, we derive a generative model that is both efficient at sampling and provides fast and explicit density estimates. We start from a parametric model represented by a neural network N_θ, and show how maximizing log-likelihood, conditioned on the network's output being a valid density, leads to the Wasserstein GAN Arjovsky et al. (2017) formulation with only minor differences. This results in an adversarial training approach whose final product is both an efficient sampling method, on the generator side, and a density estimator on the discriminator side. In doing so, we additionally propose a new architecture for the generator that combines flow models and adversarial learning. The combination of a GAN model with a flow-based generator has been explored before Grover et al. (2018). In contrast with previous work, however, our assumptions for MLE allows us to relax the requirements on the generator architecture (see Section 2.1.1). With this, we construct a flow that performs up-sampling and down-sampling operations, starting from a lower-dimensional latent variable, where density estimation of real (as opposed to generated) data points is relegated to the discriminator.

Our experimental results on sample quality, test set encoding efficiency and encoding efficiency of generated samples, show that both our new generator, and the discriminator network N_θ, work in harmony and are both of high quality (see Section 3).

In summary, our contributions are i) Our method yields a model that can compute the normalized probability density function efficiently; ii) we relax the bijectivity constraint required by traditional FLOW models, enabling more flexible generator architectures; iii) our optimization objective is closely related to that of GANs and our theoretical contributions clarify a hidden assumption made by the GAN objective. Importantly, our work provides new insight into the properties of the discriminator, which can be regarded as a density estimator with minor changes. Furthermore, it connects GANs, normalizing FLOW and EBMs from a theoretical perspective.

2 Method

Given a dataset of i.i.d samples $\mathcal{X} := \{x_i \in \mathbb{R}^n\}_{i=1}^m$, drawn from an unknown probability density P_{data}, the goal is to learn a parametric model N_θ, with parameters $\theta \in \mathcal{M}$, that matches P_{data}. Here, we represent N_θ with a neural network. To make it a valid density function, we must ensure that N_θ is positive everywhere, and that it encloses unit mass. Henceforward, we call this normalized version of N_θ as the model density P_θ and the neural network embodying N_θ as the discriminator network (or the density estimator network) because of its similarity to the discriminator of a GAN. We determine the parameters θ by maximizing the expected log-likelihood, yielding the following constrained optimization:

$$\underset{\theta \in \mathcal{M}}{\operatorname{argmax}} \sum_{x_i} log(N_\theta(x_i)) \quad s.t. \quad N_\theta(x) > 0 \; \forall x \; ; \int_{\mathbb{R}^n} N_\theta(x) dx = 1 \tag{1}$$

It is easy to ensure a positive density by setting the last activation of the neural network to an exponential function. However, the integral on the right-hand side is generally intractable and hard to compute. We can approximate this integral by using Monte Carlo sampling, and rewrite it as follows:

$$\alpha_\theta = \int_{\mathbb{R}^n} N_\theta(x) dx = \int_{\mathbb{R}^n} P_G(y) \frac{N_\theta(y)}{P_G(y)} dy = \mathbb{E}_{y \sim P_G(Y)} \frac{N_\theta(y)}{P_G(y)} \tag{2}$$

Here, $P_G(y)$ is an arbitrary density of the random variable $Y \in \mathbb{R}^n$ that is non-zero wherever the true data density $P(X)$ is non-zero and $\mathbb{E}$ represents the expectation operation. We have also assigned the shorthand α_θ for future reference to this integral. This, however, is analytically intractable. Therefore, we use a finite sample approximation of the expectation.

The problem with this method, however, is that the sample complexity is unrealistically large when $y \in \mathbb{R}^n$ and n is large. The sample efficiency can be greatly boosted by performing importance sampling, especially so, when the true data density is highly concentrated. This is widely believed to be the case with natural images, since neighboring pixels are highly correlated. Therefore, we propose the following technique to efficiently get samples $y_j = G_\phi(z_j, \eta_j)$, to compute the expectation. Here, $z_j \in \mathbb{R}^d$ is a latent vector with $d << n$, G_ϕ is the generator, which is a deterministic function that embeds the latent variable into the data space, and $\eta_j \in \mathbb{R}^{n-d}$ is auxiliary noise. We further assume a prior distribution $P(Z)$ for the latent variable z_j and an independent isotopic Gaussian distribution with variance $\sigma * I$, for the auxiliary noise η_j. Here, I denotes an identity matrix of appropriate size. This lets us efficiently approximate the expectation in Eq. 2 with $\sum_{z_j \sim P(Z), \eta_j \sim \mathcal{N}(0, \sigma * I)} [N_\theta(G_\phi(z_j, \eta_j))/P_G(Y = G_\phi(z_j, \eta_j))]$. Given this, Eq. 1 can now be rewritten as in Eq. 3

$$\begin{aligned} &\underset{\theta}{\text{argmax}} \sum_{x_i} log \left(\frac{N_\theta(x_i)}{\frac{1}{N} \sum_{z_j, \eta_j} N_\theta(G_\phi(z_j, \eta_j))/P_G(G_\phi(z_j, \eta_j))} \right) \\ &= \underset{\theta}{\text{argmax}} \sum_{x_i} \left(log(N_\theta(x_i)) - log \left(\sum_{z_j, \eta_j} \frac{N_\theta(G_\phi(z_j, \eta_j))}{P_G(G_\phi(z_j, \eta_j))} \right) \right) = \mathcal{L}_{real} + \mathcal{L}_{fake} \end{aligned} \tag{3}$$

Eq. 3 serves as our objective function for training θ. Here, we define $\mathcal{L}_{real} := log(N_\theta(x_i))$ and $\mathcal{L}_{fake} := -log(\sum_{z_j, \eta_j} N_\theta(G_\phi(z_j, \eta_j))/P_G(G_\phi(z_j, \eta_j)))$ for quick reference. Note that Eq. 3 is the same objective function as in EBMs, except that here we explicitly define the integral, or its approximation. If we approximate $\mathcal{L}_{fake}$ by a single sample of Z_j and η_j, then Eq. 3 can further be simplified, as in Eq. 4. Further, $log\, P_G(G_\phi(z_j, \eta_j))$ is not dependent on θ and hence can be dropped from this optimization. This fully recovers the usual GAN objective for the critic network.

$$\begin{aligned} &\underset{\theta}{\text{argmax}} \sum_{x_i} \left(log(N_\theta(x_i)) - log \left(\sum_{z^i} c_z^i N_\theta(G_\phi(z_j, \eta_j)) \right) \right) \\ &\approx \underset{\theta}{\text{argmax}} \sum_{x_i} \left(log(N_\theta(x_i)) - log \left(N_\theta(G_\phi(z_j, \eta_j)) \right) - log(P_G(G_\phi(z_j, \eta_j))) \right) \end{aligned} \tag{4}$$

This equation, however, requires a suitable function G_ϕ. We choose to use a neural network to represent this function, and let us call this network the generator network. To compute $\mathcal{L}_{fake}$, clearly one needs to have access to $P_G(Y)$ evaluated at $y_j = G_\phi(z_j, \eta_j)$ for arbitrary z_j and η_j. We could in principle obtain this by using normalizing flows as the generator, but this would impose strong restrictions on the architecture. Specifically, this would require the whole network to be analytically invertible, and consequently the latent space cannot be of lower dimensionality than the input data. However, note that in our case we can relax this requirement, since we only need to evaluate $P_G(Y)$ at points that have the form $y_j = G_\phi(z_j, \eta_j)$, i.e., only at generated points. We discuss how to construct such a flow in Section 2.1.1.

2.1 Generator objective

Before diving deep in to the details of the generator architecture, it is worth examining the objective function with which we intend to optimize the parameters of it. A quick inspection of Eq. 2 shows that it has the form of the importance sampling mechanism. In such scenarios, often the biased distribution ($P_G(Y)$ in our case) is chosen such that the variance of the weighted samples is reduced Rubinstein and Kroese (2016). In our case, the variance of $\frac{N_\theta(y)}{P_G(y)}$ is minimized if we match $N_\theta(y)$ and $P_G(y)$ up to a multiplicative factor, more precisely $P_G(y) = N_\theta(y)/\alpha_\theta$, everywhere. Here, α is the integral constant and is not known precisely. We do so by minimizing a divergence measure between $P_G(Y)$ and $N_\theta(Y)$. Here, $N_\theta(Y)$ as usual, represents the unnormalized density that we seek

to fit to our training data. We choose the KL divergence measure Kullback and Leibler (1951). We do so specifically because, as seen from Eq. 5, the optimization for the generator parameter becomes independent of the normalizing constant of the distribution given by N_θ.

$$\begin{aligned}&\underset{\phi}{\operatorname{argmin}}\, \mathbb{E}_{y_i \sim P_G(Y)} log\left(\frac{P_G(y_i)\alpha_\theta}{N_\theta(y_i)}\right) = \underset{\phi}{\operatorname{argmax}}\, \mathbb{E}_{y_i \sim P_G(Y)}[-logP_G(y_i) + logN_\theta(y_i) - log\alpha_\theta] \\ &= \underset{\phi}{\operatorname{argmax}}\, \left[H(P_G(Y)) + \mathbb{E}_{z_i \sim P(Z)} logN_\theta(G_\phi(z_i))\right]\end{aligned} \tag{5}$$

Here $H(P_G(Y))$ represents the entropy of the generator distribution. A close look at Eq. 5 reveals that it is identical to the generator objective of a Wasserstein-GAN Arjovsky et al. (2017) except for the additional entropy term. This term precisely seeks to increase diversity of the generated samples.

2.1.1 Generator function using a non-invertible flow

To take advantage of the above-mentioned relaxed requirement of our generator function G_ϕ we propose a variant of normalizing-flow networks. In fact, in this type of network we neither maintain dimensionality nor invertibility, therefore strictly speaking they are not flow networks. These networks are composed of layers of simple functions that operate on a random variable to produce a transformed random variable, such that given the density of the input random variable, we can efficiently compute the density of the output random variable. For this purpose, we borrow the change of variable mechanism, formally described in Eq. 6. The difference between our network and traditional normalizing-flow networks is that our model neither needs to be efficiently invertible, nor does it always preserve dimensionality. We can both increase and decrease dimensionality. This ability precisely let us build architectures close to modern GAN architectures, which have heuristically been found to work well. Note that, in exchange, we cannot compute probabilities for random images – only for generated ones. In our framework, this function is provided by the discriminator instead.

2.1.2 Increasing dimensionality

Given a function $t = g(u) : \mathbb{R}^o \rightarrow \mathbb{R}^o$, the change of variable formula dictates that $P(T) = P(U)\left|\frac{\partial g}{\partial u}\right|^{-1}$. A multi-layer neural network, e.g., our generator G with l layers, can be thought of as a series of operations; i.e., $G := g_1(g_2(g_3(...g_l(.))))$, formally, $t_1 = g_1(u_1), t_2 = g_2(u_2),\ ...\ t_l = g_l(u_l)$, and $t_2 = u_1, t_3 = u_2,\ ...\ t_l = u_{l-1}$. In such a scenario, if $t_1, t_2, t_3\ ...\ t_l, u_1, u_2, u_3,\ ...\ u_l \in \mathbb{R}^o$, one can track the density of the activations as follows in Eq. 6

$$P(t_k) = P(u_k)\left|\frac{\partial g_k}{\partial u_k}\right|^{-1} \quad \forall k \in \{1\ ...\ l\} \tag{6}$$

A sufficient criterion for this to remain valid is bijectivity of, $g_k \forall k$ and that, in turn, enforces the dimensionality of z_k and a_k to be equal. However, we are free to redefine $t_k := [u_{k-1}||an_k]$. Here, '||' represents a concatenation operation and $\eta_j \sim \mathcal{N}(0, I)$, where $\mathcal{N}$ is the normal distribution with mean zero and identity variance. This enables us to introduce noise at multiple layers of operation in the generator and, starting from a low-dimensional latent space, generate high-dimensional data, similar to StyleGAN Karras et al. (2019). This modification and Eq. 6 enables us to write Eq. 7

$$P(t_{k+1}) = P(t_k)\left|\frac{\partial g_k}{\partial t_k}\right|^{-1} P(an_k)\ \ \forall k \in \{1\ ...\ l\} \tag{7}$$

2.1.3 Dimensionality reduction

To closely follow traditional generator architecture, e.g., the DC-GAN architecture Radford et al. (2015), one necessary operation is dimensionality reduction, i.e., to have operations of the form $t_k = g_k(u_k) : \mathbb{R}^{o_1} \rightarrow \mathbb{R}^{o_2}\ ; o_1 > o_2$. Moreover, to compute $\mathcal{L}_{fake}$, given the density of the input random variable $P(U_k = u_k)$, one must be able to efficiently compute the density of the output random variable $P(T_k = g_k(u_k))$. For the time being, imagine that $t_k \in \mathbb{R}^{o_2}$, i.e., g_k is a dimensionality preserving operation. Now, let us group t_k in two parts, i.e., $t_k = [t_k^1||t_k^2]$. Here, '||' represents the concatenation operation and $t_k^1 \in \mathbb{R}^{o_2}, t_k^2 \in \mathbb{R}^{o_1 - o_2}$. In such a setting, a dimensionality reduction

operation would simply ignore t_k^2 and recover a function between $\mathbb{R}^{o_1} \rightarrow \mathbb{R}^{o_2}$. Any such function, however, requires us to compute $P(T_k^1 = t_k^1)$ given $P(T_k = t_k) := P(T_k = [t_k^1|t_k^2]) := P(T_k^1, T_k^2)$. This is a marginalization operation and can be computed as $\int_{T_k^2} P(T_k^1, T_k^2) dT_k^2$. This integral is unfortunately intractable in the general case. Therefore, we make a case-specific assumption, namely, we assume that, in real images, a pixel is normally distributed given its immediate neighbor. This assumption lets us marginalize T_k^2 efficiently, as shown in Eq. 8

$$P(T_k^1) = \frac{P(T_k^1, T_k^2)}{P(T_k^2|T_k^1)} = \frac{P(T_k^1, T_k^2)}{\mathcal{N}(T_k^1, \sigma * I)} \tag{8}$$

Here in Eq. 8, we get the second equality using our assumption stated above, σ represents a tunable variance of the normal distribution, and I is an identity matrix.

2.2 Tailoring the candidate density function

We chose to represent N_θ, with a deep neural network. A deep neural network is a composition of repeated linear projection operations with nonlinear activations. Furthermore, often the linear operations, e.g., strided convolution, reduce dimensions by projecting the input vector to a subspace. These operations hope to retain the most 'useful' dimensions for the task at hand. In our case, the network is encouraged to produce high responses for points coming from a dataset. Therefore, the linear layers are expected to align themselves to the axis of the highest data variance. Now, if we use this network for points that do not come from our training data set or are not even are of the same kind, e.g., non images, they are expected to have significant variance on axes different from the high-variance axes of the data. We can exploit this feature, to assign low probability to such samples. Concretely, a linear operation with weight matrix w operating on a data vector x can be expressed as a matrix vector multiplication $t_\parallel = w * x$. Here $t_\parallel$ is the component of x in the subspace spanned by the rows [2] of w. We can recover the component perpendicular to this subspace [3] $t_\perp = x - \frac{t_\parallel^T * w}{||t_\parallel^T * w||_2} * x$. Here, $\{\cdot\}^T$ represents the transpose operation and $||\cdot||_2$ represents the vector norm operation. As discussed above, we expect this perpendicular component $t_\perp$ to be large for points that do not belong to our training data and therefore should be assigned low density. Therefore our density network is evaluated as $N_\theta(x)e^{-\sum_k ||t_{\perp k}||_2}$. Here $t_{\perp k}$ represents the perpendicular component at every linear projection layer.

2.3 Architecture

LED consists of a generator and a discriminator. The discriminator in our case plays the role of a density estimator. As described in Section 2.1, the generator consists of l transformations given by $g_k \; ; \; k \in \{1, 2, 3...l\}$. We choose these transformations carefully such that, given the density of the input variable, we can efficiently compute the density of the output variable. A traditional GAN architecture often employs fully connected, convolution, batch normalization, ReLU and interpolation layers. We implement a mechanism to keep track of the probability density through all of these operations; precise implementation details can be found in the supplementary material, Section C. Our final generator architecture closely follows that of DCGAN Radford et al. (2015), known to perform well with adversarial training. The discriminator architecture follows precisely that of DCGAN, except that we subtract the perpendicular component in the convolution layers (Section 2.2).

3 Experiments

In this section, we provide experimental results for the generated data and the density estimation using both synthetic (Section 3.1) and real (Section 3.2) datasets. We show qualitative examples in Section 3.3. Implementation details can be found in the Sup. Mat., Section B.1.

[2] considering x is a column vector.

[3] assuming that w is row rank deficient.

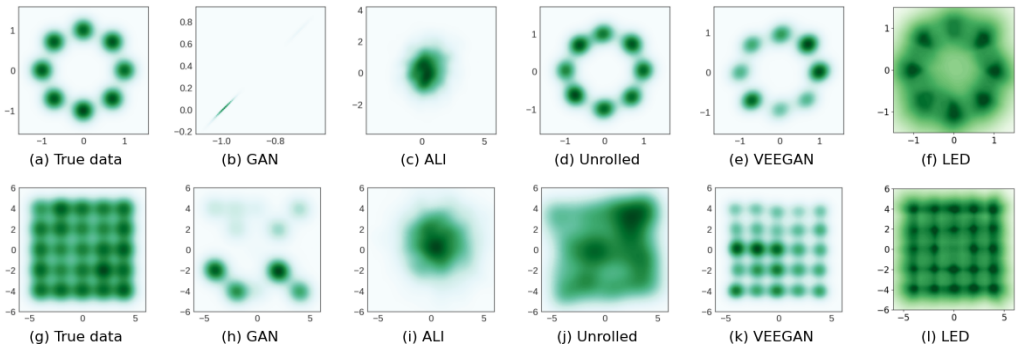


Figure 1: Density modeled by different generative models. Top row: Ring of Gaussians. Bottom row: Grid of Gaussians. (a-e,g-k) are taken from Srivastava et al. (2017) and were produced by kernel density estimation run on generated samples. (f,l) the direct density (in log scale) computed by LED. Note that our model assigns a non-zero probability to regions where the KDE does not, since only a finite number of samples were used to estimate generator density in the experiments (a-e,g-k).

3.1 Synthetic Data

We begin by examining the notion of data distribution captured by our **discriminator** model (i.e., density estimator), compared to other GAN-based methods. To this end, we perform an experiment on a toy 2D dataset, similar to the one presented in VEEGAN Srivastava et al. (2017). In particular, we train our model on two sets of Gaussian Mixture Models (GMM), with one set comprising 8 modes forming a ring (Fig. 1a) and another set comprising 25 modes in a grid (Fig. 1g).

Since GAN models normally do not return a direct estimate of the probability of the data, the compared methods use Kernel Density Estimation (KDE) to visualize the relevant probability, as shown in Fig. 1(a-e, g-k). Note that LED instead has direct access to this value through the discriminator. We observe that the density learned by LED (shown in Fig. 1(a-e, g-k)) matches the true distribution, returning high probability for all modes, and low probability away from them.

We also quantify the quality of the density captured by the **generator**. For this, we use the High-Quality Samples metric from Srivastava et al. (2017), where a generated point is considered *high quality* if it is within a 3σ distance from the nearest mode. We generate 2,500 points and report the percentage of points that are high quality over five runs. We can see here (in table 1) that our generator produces significantly higher quality samples than other models, achieving 10% more than VEEGAN Srivastava et al. (2017). On the other hand, our model is not capable of fully capturing all 25 modes in the second GMM. We hypothesize that this is due to an insufficient expressive power of the generator. To test this hypothesis, we follow this following experiment protocol. First, with an intentionally weakened generator, we capture a smaller number of modes. We find that this is consistent and reproducible. Next, when we progressively increase the power of the generator, we see that our model progressively generates more modes. The result of this experiment, along with qualitative results for the generator density, can be found in the Sup. Mat., Section E.1.

3.2 Real Data

We now show results of LED over real data generation, where we compare against the flow-based model GLOW Kingma and Dhariwal (2018), and a GAN baseline that uses our same architecture, but with a standard GAN loss Kingma and Welling (2014). We also compare the results of different numbers of samples for the integration approximation. We train these models with the MNIST Deng (2012) and CelebA Liu et al. (2015) datasets and evaluate the results using (1) Fréchet Inception Distance (FID), and (2) bits-per-pixel (b/p) of the test set. We compute the b/p of real images by computing their negative-log-likelihood using the score given by the discriminator along with Eq. 2, and subsequently normalizing the result by the number of pixels D : $b/p = \frac{1}{n}\sum_{x\in X}\frac{d(x)}{\alpha_0 D \ln 2}$. We also compute the b/p for the generated images using the discriminator score and the generator probability. For the discriminator score, we use the same method as with the real images. For the

	2D Ring		2D Grid	
	Modes (Max 8)	**% HQ Samples**	**Modes (Max 25)**	**% HQ Samples**
GAN Goodfellow et al. (2014)	1	99.3	3.3	0.5
ALI Dumoulin et al. (2017)	2.8	0.13	15.8	1.6
Unrolled GAN Metz et al. (2017)	7.6	35.6	23.6	16
VEEGAN Srivastava et al. (2017)	**8**	52.9	**24.6**	40
LED (ours)	**8**	**63.5**	16.2	**68.3**

Table 1: The high quality (HQ) samples percentages of various generators for 2D GMMs. The numbers for all models, except LED (ours), are taken from Srivastava et al. (2017). LED produces higher quality samples than all other tested models. Here, high-quality samples are defined to be samples are within 3σ of a real data mode.

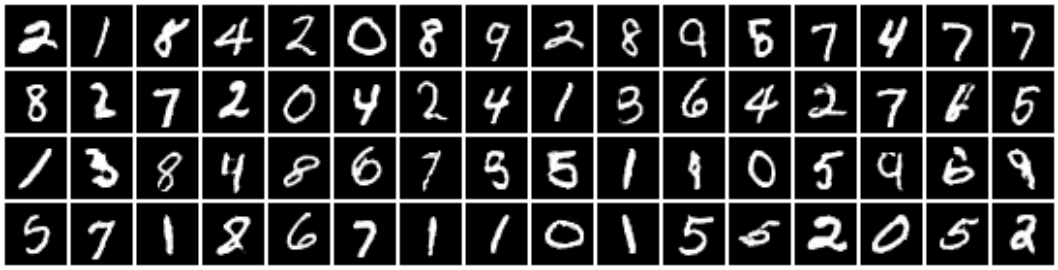


Figure 2: Random examples of generated images using MNIST at 32 × 32 resolution. FID 4.19.

generator b/p we use the change of variables formula, as we know the latent vector and its probability along with the log-determinant of the generator's Jacobean: $\ln P_g\left(G\left(z\right)\right) = \ln P\left(z\right) - \ln \left|\frac{\partial G(z)}{\partial z}\right|$.

Generated samples can be seen in Fig. 2 for MNIST dataset and in Fig. 3 for CelebA dataset. The corresponding FID and b/p results are reported in Tbl. 2. LED outperforms the current state of the art in terms of b/p metric, which increases with the number of samples used for the integral approximation. Looking at the FID scores, we see that using only one sample results in unrealistic images (high FID). This is understandable since this approach is equivalent to training a generator with only a single sample for every batch of the discriminator, which has been observed to perform poorly Brock et al. (2019). Increasing the number of samples significantly improves the FID scores to comparative values with the state of the art. Tbl. 2 also shows that subtracting the perpendicular part (Sec. 2.2) in the discriminator (Section 2.2) results in a better quality image (lower FID) and better efficiency (lower b/p).

3.3 Qualitative Results

In Fig. 4 (and in Section E.2 in Sup. Mat.) we visually assess the probabilities assigned by the discriminator by showing random samples sorted by density. We can see here that high quality images get higher probabilities than low quality images, suggesting that our trained discriminator correctly captures the distribution of the given dataset.

We also demonstrate the power of the discriminator by optimizing over its score. We begin by generating images using latent vectors that are between 1.5 and 3σ away from the origin, which are usually of low quality. We then optimize the latent vectors such that they maximize the output of the discriminator. The results, in the supplementary material, Section E.4 show that this approach can significantly increase the quality of the images for MNIST.

Finally, we show in Fig. 5 (and in Section E.3 in Sup. Mat.) qualitative results for the generator on an interpolation experiment.



Figure 3: Random examples of generated images using CelebA at 64×64 resolution. FID 12.6.

Model	MNIST			CelebA		
	FID	b/p	smpl b/p	FID	b/p	smpl b/p
DC-GAN	5.6	–	–/–	(12.5)13	–	–/–
GLOW	11	–	–/–	–	–	–/–
Ours-1sa	118	0.509	1.011 / 8.245	209	0.019	0.025/2.366
Ours-64sa	4.3	0.546	0.992 / 8.75	24	0.009	0.012/1.049
Ours-256sa	4.19	0.530	1.003 / 8.515	36	0.022	0.022/0.012

Table 2: FID and bits-per-pixel (b/p) of the held-out test set, and b/p of the generated samples. Note that the latter can be evaluated using our flow-based generator, as well as the independent density estimator network; we report them as *generator* b/p */ critic* b/p. Here, 64sa, 256sa stands for the number of samples used to approximate the second sum of Eq. 3. The GLOW b/p and FID for CelebA could not be calculated since it failed to converge with default parameter settings.

4 Related work

Two main categories of generative models are *prescribed* and *implicit* models Diggle and Gratton (1984). Prescribed models recover an explicit parametric specification of the density function and are trained and evaluated by maximum likelihood estimation (MLE); our work belongs to this family. Implicit models, on the other hand, represent the data distribution indirectly through a stochastic mechanism that generates random samples. In general, this offers more flexibility in terms of learning objective and model architecture, which is hypothesized to be responsible for the high visual quality of the generated samples.

Normalizing flows Kobyzev et al. (2020); Dinh et al. (2016); Kingma and Dhariwal (2018) and autoregressive models Theis and Bethge (2015); Van den Oord et al. (2016b); Salimans et al. (2017) are examples of deep *prescribed* generative models. Since these compute the density function explicitly, they can be optimized and evaluated using the train and test-set log-likelihood. Although autoregressive models can efficiently work with high-dimensional data during training, due to ancestral sampling they are extremely slow at generating new samples. Normalizing flows require an invertible architecture to compute the likelihood, and consequently can only support latent spaces of the same dimensionality as the input data. In addition, they tend to yield large and memory-hungry models, and are therefore not so suitable for high-dimensional data. In this work, we relax the invertibility constraint by computing the flow in only one direction, enabling the use of lower-dimensional latent vectors, and more computational resource efficient architectures.

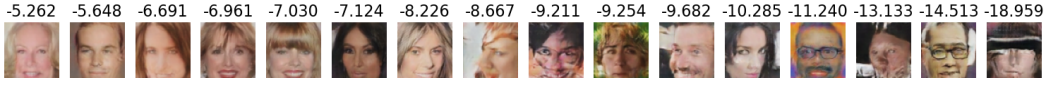


Figure 4: Random samples of generated images with their discriminator-assigned probability above.



Figure 5: Generated images from linear interpolations of the latent space, using the CelebA dataset.

Generative Adversarial Networks (GANs) are the most prominent example of *implicit* models. GANs currently produce state-of-the-art generated sample quality Karras et al. (2020). However, it has been observed that GANs may trade diversity for precision Che et al. (2016); Salimans et al. (2016); Srivastava et al. (2017). This results in generators that produce samples from only a few modes of the data distribution, a phenomenon known as 'mode collapse'. GANs are also well known for having unstable training dynamics Arjovsky et al. (2017); Mescheder et al. (2018); Heusel et al. (2017).

An intermediate category of generative models considers only an *approximation* to the density function. Examples include a lower bound on the likelihood for VAEs Kingma and Welling (2014) and diffusion models Ho et al. (2020), or the unnormalized density in the case of EBMs Song and Kingma (2021). VAEs are known to suffer from low generation quality, i.e., they tend to produce blurry samples. Diffusion models can generate images of very high sample-quality Dhariwal and Nichol (2021); however, the latent representation needs to be of the same dimension as the input data. EBMs deploy several techniques to obtain the derivative of the normalizing factor with respect to the model parameters. We maximize the same cost function as EBMs (see Eq. 1), but explicitly model the normalization constant α_θ. As explained in Section 2, this leads to a variant of the GAN formulation, thus making connections between the three models.

5 Conclusion

We presented a new generative model, LED, which is closely related to GANs while being able to efficiently compute the density function of the data. Our formulation, based on maximizing log-likelihood of the discriminator output, recovers a training objective that is similar to the objective function of GANs, but with a crucial difference that introduces an entropy maximization term in the generator objective. Our experimental results show that LED produces a generator that is on par with other GAN generators, along with accurate density estimations. LED provides new understandings on the properties of the discriminator, and provides insights into GANs from a maximum likelihood perspective, while connecting these with EBMs. We believe this can open up promising directions into understanding and improving generative models.

References

Arjovsky, M., Chintala, S., and Bottou, L. (2017). Wasserstein Generative Adversarial Networks. In *International inproceedings on Machine Learning (ICML)*.

Brock, A., Donahue, J., and Simonyan, K. (2019). Large scale GAN training for high fidelity natural image synthesis. In *International Conference on Learning Representations*.

Che, T., Li, Y., Jacob, A. P., Bengio, Y., and Li, W. (2016). Mode regularized generative adversarial networks. *arXiv preprint arXiv:1612.02136*.

Deng, L. (2012). The mnist database of handwritten digit images for machine learning research. *IEEE Signal Processing Magazine*.

Dhariwal, P. and Nichol, A. (2021). Diffusion models beat gans on image synthesis. *Advances in Neural Information Processing Systems*, 34.

Diggle, P. J. and Gratton, R. J. (1984). Monte Carlo Methods of Inference for Implicit Statistical Models. *Journal of the Royal Statistical Society: Series B (Methodological)*.

Dinh, L., Krueger, D., and Bengio, Y. (2014). Nice: Non-linear Independent Components Estimation. *arXiv preprint arXiv:1410.8516*.

Dinh, L., Sohl-Dickstein, J., and Bengio, S. (2016). Density Estimation Using Real NVP. *arXiv preprint arXiv:1605.08803*.

Dumoulin, V., Belghazi, I., Poole, B., Lamb, A., Arjovsky, M., Mastropietro, O., and Courville, A. C. (2017). Adversarially learned inference. In *5th International Conference on Learning Representations, ICLR 2017, Toulon, France, April 24-26, 2017, Conference Track Proceedings*. OpenReview.net.

Goodfellow, I., Pouget-Abadie, J., Mirza, M., Xu, B., Warde-Farley, D., Ozair, S., Courville, A., and Bengio, Y. (2014). Generative Adversarial Nets. In *Advances in Neural Information Processing Systems (NeurIPS)*.

Grover, A., Dhar, M., and Ermon, S. (2018). Flow-GAN: Combining Maximum Likelihood and Adversarial Learning in Generative Models. In *Proceedings of the AAAI inproceedings on Artificial Intelligence*.

Heusel, M., Ramsauer, H., Unterthiner, T., Nessler, B., and Hochreiter, S. (2017). GANs Trained by a Two Time-scale Update Rule Converge to a Local Nash Equilibrium. *Advances in Neural Information Processing Systems (NeurIPS)*.

Ho, J., Jain, A., and Abbeel, P. (2020). Denoising Diffusion Probabilistic Models. In *Advances in Neural Information Processing Systems (NeurIPS)*.

Huber, P. (1967). The behavior of maximum likelihood estimates under nonstandard conditions. In *Proceedings of the Fifth Berkeley Symposium on Mathematical Statistics and Probability*. University of California Press.

Karras, T., Laine, S., and Aila, T. (2019). A style-based Generator Architecture for Generative Adversarial Networks. In *Proceedings of the IEEE inproceedings on Computer Vision and Pattern Recognition (CVPR)*.

Karras, T., Laine, S., Aittala, M., Hellsten, J., Lehtinen, J., and Aila, T. (2020). Analyzing and Improving the Image Quality of StyleGAN. In *Proceedings of the IEEE inproceedings on Computer Vision and Pattern Recognition (CVPR)*.

Kingma, D. P. and Ba, J. (2015). Adam: A Method for Stochastic Optimization. In *3rd International Conference on Learning Representations, ICLR 2015, San Diego, CA, USA, May 7-9, 2015, Conference Track Proceedings*.

Kingma, D. P. and Dhariwal, P. (2018). Glow: Generative flow with invertible 1x1 convolutions. In Bengio, S., Wallach, H., Larochelle, H., Grauman, K., Cesa-Bianchi, N., and Garnett, R., editors, *Advances in Neural Information Processing Systems*, volume 31. Curran Associates, Inc.

Kingma, D. P. and Welling, M. (2014). Auto-Encoding Variational Bayes. In *International inproceedings on Learning Representations (ICLR)*.

Kobyzev, I., Prince, S., and Brubaker, M. (2020). Normalizing Flows: An Introduction and Review of Current Methods. In *IEEE Transactions on Pattern Analysis and Machine Intelligence (PAMI)*.

Kullback, S. and Leibler, R. A. (1951). On Information and Sufficiency. *The annals of mathematical statistics*.

Liu, Z., Luo, P., Wang, X., and Tang, X. (2015). Deep learning face attributes in the wild. In *Proceedings of the IEEE international conference on computer vision*.

Mescheder, L., Geiger, A., and Nowozin, S. (2018). Which training methods for GANs do actually converge? In *International inproceedings on Machine Learning (ICML)*.

Metz, L., Poole, B., Pfau, D., and Sohl-Dickstein, J. (2017). Unrolled generative adversarial networks. In *5th International Conference on Learning Representations, ICLR 2017, Toulon, France, April 24-26, 2017, Conference Track Proceedings*. OpenReview.net.

Radford, A., Metz, L., and Chintala, S. (2015). Unsupervised Representation Learning with Deep Convolutional Generative Adversarial Networks. *arXiv preprint arXiv:1511.06434*.

Rubinstein, R. Y. and Kroese, D. P. (2016). *Simulation and the Monte Carlo Method*. John Wiley & Sons.

Salimans, T., Goodfellow, I., Zaremba, W., Cheung, V., Radford, A., and Chen, X. (2016). Improved techniques for training gans. *Advances in neural information processing systems*, 29.

Salimans, T., Karpathy, A., Chen, X., and Kingma, D. P. (2017). PixelCNN++: Improving the PixelCNN with Discretized Logistic Mixture Likelihood and other Modifications. In *International inproceedings on Learning Representations (ICLR)*.

Sedghi, H., Gupta, V., and Long, P. M. (2019). The Singular Values of Convolutional Layers. In *International inproceedings on Learning Representations (ICLR)*.

Song, Y. and Kingma, D. P. (2021). How to train your energy-based models. *arXiv preprint arXiv:2101.03288*.

Srivastava, A., Valkov, L., Russell, C., Gutmann, M. U., and Sutton, C. (2017). VEEGAN: Reducing Mode Collapse in GANs Using Implicit Variational Learning. *Advances in Neural Information Processing Systems (NeurIPS)*.

Theis, L. and Bethge, M. (2015). Generative Image Modeling Using Spatial LSTMs. In *Advances in Neural Information Processing Systems (NeurIPS)*.

Van den Oord, A., Kalchbrenner, N., Espeholt, L., Vinyals, O., Graves, A., et al. (2016a). Conditional Image Generation with PixelCNN Decoders. *Advances in Neural Information Processing Systems (NeurIPS)*.

Van den Oord, A., Kalchbrenner, N., and Kavukcuoglu, K. (2016b). Pixel Recurrent Neural Networks. In *International inproceedings on Machine Learning (ICML)*.

Checklist

The checklist follows the references. Please read the checklist guidelines carefully for information on how to answer these questions. For each question, change the default **[TODO]** to [Yes] , [No] , or [N/A] . You are strongly encouraged to include a **justification to your answer**, either by referencing the appropriate section of your paper or providing a brief inline description. For example:

- Did you include the license to the code and datasets? [Yes] In Sup. Mat.
- Did you include the license to the code and datasets? [No] The code and the data are proprietary.

- Did you include the license to the code and datasets? [N/A]

Please do not modify the questions and only use the provided macros for your answers. Note that the Checklist section does not count towards the page limit. In your paper, please delete this instructions block and only keep the Checklist section heading above along with the questions/answers below.

1. For all authors...
   (a) Do the main claims made in the abstract and introduction accurately reflect the paper's contributions and scope? [Yes]
   (b) Did you describe the limitations of your work? [No]
   (c) Did you discuss any potential negative societal impacts of your work? [No]
   (d) Have you read the ethics review guidelines and ensured that your paper conforms to them? [Yes]
2. If you are including theoretical results...
   (a) Did you state the full set of assumptions of all theoretical results? [Yes]
   (b) Did you include complete proofs of all theoretical results? [Yes]
3. If you ran experiments...
   (a) Did you include the code, data, and instructions needed to reproduce the main experimental results (either in the supplemental material or as a URL)? [Yes]
   (b) Did you specify all the training details (e.g., data splits, hyperparameters, how they were chosen)? [Yes]
   (c) Did you report error bars (e.g., with respect to the random seed after running experiments multiple times)? [No]
   (d) Did you include the total amount of compute and the type of resources used (e.g., type of GPUs, internal cluster, or cloud provider)? [No]
4. If you are using existing assets (e.g., code, data, models) or curating/releasing new assets...
   (a) If your work uses existing assets, did you cite the creators? [Yes]
   (b) Did you mention the license of the assets? [Yes]
   (c) Did you include any new assets either in the supplemental material or as a URL? [Yes]
   (d) Did you discuss whether and how consent was obtained from people whose data you're using/curating? [No]
   (e) Did you discuss whether the data you are using/curating contains personally identifiable information or offensive content? [No]
5. If you used crowdsourcing or conducted research with human subjects...
   (a) Did you include the full text of instructions given to participants and screenshots, if applicable? [N/A]
   (b) Did you describe any potential participant risks, with links to Institutional Review Board (IRB) approvals, if applicable? [N/A]
   (c) Did you include the estimated hourly wage paid to participants and the total amount spent on participant compensation? [N/A]

Appendices

A Change of variable

As described in Section 2.1.2, we need to keep track of the density of the input random variable as it passes through different layers of the generator. In our architecture we used fully connected, convolutional, batch norm, dimensionality inflation, and an activation layer. We describe in the following each of these layers, how to estimate the output density given the input density, and how to compute the determinant of the Jacobian.

A.1 Fully connected

A fully connected layer can be represented as

$$t = wu + b \tag{9}$$

Here $u \in \mathbb{R}^{o_1}$ is the input variable, $w \in \mathbb{R}^{o_1 \times o_1}$ is a square weight matrix, and $b \in \mathbb{R}^{o_1}$ is the bias vector. To compute the output density using the change of variable formula, we simply compute the log determinant of the weight matrix using PyTorch's *slogdet()* function. One must ensure w to be full rank in order for the change of variable formula to still apply. However, since our objective is to maximize entropy of the generator and therefore maximize the absolute determinant, a good initialization ensures w to have full rank.

A.2 Activation

Since ReLU is not an invertible operation, it is not suitable to use it in our generator. However, several modern generator architectures use ReLU, and it has been shown to improve performance of neural networks empirically. Therefore, we design our own activation function that closely follows ReLU and yet is suitable for our use case. We define our custom activation as:

$$L(u) = \frac{1}{\alpha} \log \left(e^{\alpha(u-u_0)} + e^{\beta(u-u_0)} \right) - t_0 \tag{10}$$

Where α and β are user-defined and u_0 and t_0 are offsets. We set $\alpha = 5.8$ and $\beta = 1$ (Fig. 6). This activation results in a constant slope of 1 in the positive domain. In the negative domain, the slope and elbow can be controlled by adjusting α and β. Since the activation applies to every component of its input vector independently, the Jacobian of this layer is a diagonal matrix. In the case of diagonal matrices, the log determinant is easily computed as the sum of the logarithm of each element's derivative. The derivative of each element can be easily calculated as:

$$\frac{\mathrm{d}L\left(u\right)}{\mathrm{d}u} = \frac{e^{\alpha(u-u_0)} + \frac{\beta}{\alpha} e^{\beta(u-u_0)}}{e^{\alpha(u-u_0)} + e^{\beta(u-u_0)}} \tag{11}$$

A.3 Convolution

The naive method to compute the determinant of the Jacobian of a convolutional layer would be to compute the determinant of the corresponding Toeplitz matrix of the convolution kernel. As the layers keep increasing in size, so do the Toeplitz matrices, and computing their determinant becomes a slow task. To avoid this, we use the method described by Sedghi et al. (2019) to compute the singular values and the determinant of the convolution. Their algorithm uses the fact that the circulant matrices are diagonalized by the Fourier transform. As a result, we are constrained to use convolution with circular padding. With that small change, we can compute the log determinant quickly.

A.4 Batch-norm

We take this layer verbatim from Dinh et al. (2016) as

$$B\left(u\right) = \frac{u - \mathrm{E}\left[u\right]}{\sqrt{\mathrm{Var}\left[u\right] + \epsilon}} \times \gamma + \beta \tag{12}$$

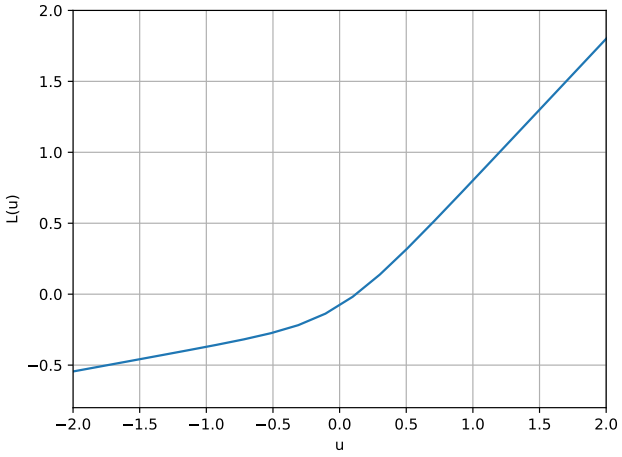


Figure 6: Our custom activation function as described in Eq. 10 with $\alpha = 5.8$ and $\beta = 1$.

Note that $\mathrm{E}[u]$ and $\mathrm{Var}[u]$ are function of all elements in u. Therefore, the Jacobian is not diagonal and is in general hard to compute. In our current implementation, we disregarded the fact that $\mathrm{E}[u]$ and $\mathrm{Var}[u]$ are functions of u and treated them as constants. As a results, the Jacobian is diagonal with each element being the simple derivative:

$$\frac{\mathrm{d}B(u)}{\mathrm{d}u_i} = \frac{\gamma}{\sqrt{\mathrm{Var}[u] + \epsilon}} \tag{13}$$

A.5 Dimensionality inflation

As described in Section 2.1.2, we increase dimensionality by introducing noise and copying over the left neighbor in an image, emulating the nearest neighbor interpolation. One can also device bi-linear or bi-cubic interpolation methods. This, however, is left as future work.

B Implementation

B.1 Implementation Details

We trained the generator and discriminator using the PyTorch ADAM optimizer Kingma and Ba (2015). The learning rate for both generator and discriminator was set to 1e-3. We trained LED on the MNIST Deng (2012) and CelebA Liu et al. (2015) datasets for 500 epochs. We saved the models after every epoch and presented the result of the epoch with the highest FID.

B.2 Perpendicular convolution

In Section 2.2, we described how one might help the density estimation function N_θ assign low density to off-the-image manifold points. The computation of the perpendicular input component in case of linear layer is shown in Section 2.2. When this linear operation is implemented using convolutions, one can perform transposed convolution to compute $t^T * w$, where t and w are as defined in Section 2.2. Importantly, however, we still have to 'lift' the dimensionality of the generated samples to the dimension of the input data dimension (number of pixels in case of images). The reason behind this 'lifting' is that data embedded in a higher-dimensional manifold is a curve without width. Having no width essentially means that the density function is a Dirac delta function over this curve Since the the Dirac delta function has no gradients outside of the embedded curve, learning such a function using gradient descent is ill-posed.

B.3 Generator: Random sampling from a Gaussian

During training, we set the generator in such a way that for each sample in a batch, with some probability, the values of its corresponding output will be replaced by samples from a normal distribution. Adding this Normal sampling defines a non-zero probability distribution over the codomain of the generator, since for each point the generator cannot generate on its own, the normal distribution has a non-zero probability.

B.4 Numerical stability in generator loss

In our experiments we found that the two terms in Eq. 5 have different orders of magnitude. This difference prevented the optimization to converge. We solved this disparity by adding a weight coefficient k to the entropy term $H(P_G(Y))$ to scale it down. In practice, this changes our KL-divergence into f-divergence with $f(t) = t \log\left(t^k\right)$. In comparison, KL-divergence is a special case of f-divergence with $f(t) = t \log(t)$.

Looking again at Eq. 5 with the new divergence formulation, $N_\theta(y_i)$ should be reformulated as $N_\theta^k(y_i)$. Instead, we redefine our discriminator's output to be $k \log N_\theta(y_i)$. With this redefinition we maintain the stability of the generator loss while not affecting the discriminator loss, since k will be implicitly computed in the integral approximation of Eq. 2.

C Architecture

C.1 DC-GAN based

The generator architecture we used for MNIST and CelebA is based on the DC-GAN architecture. Given a latent vector, the generator first increases the dimensionality by using a linear layer which is then padded with noise. The size of the hidden latent image is then doubled on the expense of the number of channels multiple times, until the number of channels reaches the target number (1 for MNIST, 3 for CelebA). The image is then down-sampled (Section 2.1.3) until it reaches the required number of pixels.

C.2 Expressive power of the generator for a toy problem

For the 2D synthetic data (Section 3.1) we follow the same principles as in Section C.1, but with slight differences. The generator receives as input a 2D point. This 2D point is expanded to have the maximal number of features by the use of linear layers, where each linear layer doubles the number of features. The maximal number of features is defined by the user before initialization After the expansions, the resulting latent vector goes through a number of blocks, where each block contains a linear layer that maintains dimensionality, a batch normalization layer and an activation function. The number of blocks is defined by the user before initialization. For the results shown in the paper we used 256 features and 8 blocks. The result is then down-sampled (Section 2.1.3) until it is 2D.

In Section 3.1 we showed that our generator could not capture all the modes. We believe that this was caused by the fact that the generator architecture was not expressive enough for the task. To support this, the effects of different maximal number of features and number of blocks are shown in Section E.1. We can see that with a smaller number of blocks the generator can capture more modes. Theoretically, with a large number of blocks the generator could capture more modes, albeit with very long computation times. In the future we will look into ways to increase the expressive power of the generator without excessively increasing the computational time.

D Approximation quality of the integral

In order to see how many samples are required and how the training time affects the approximation, we compared the approximated α_θ across two models, one trained with 1 sample and the other with 256 samples. After training each model for a certain number of epochs, we approximated α_θ with a different number of samples. We calculated α_θ 20 times for each model and epoch, and report the means and standard deviations in Fig. 7. Fig. 7 shows us that when training the model with 256 samples (left column), α_θ converges to a constant value across epochs (about 185), with the

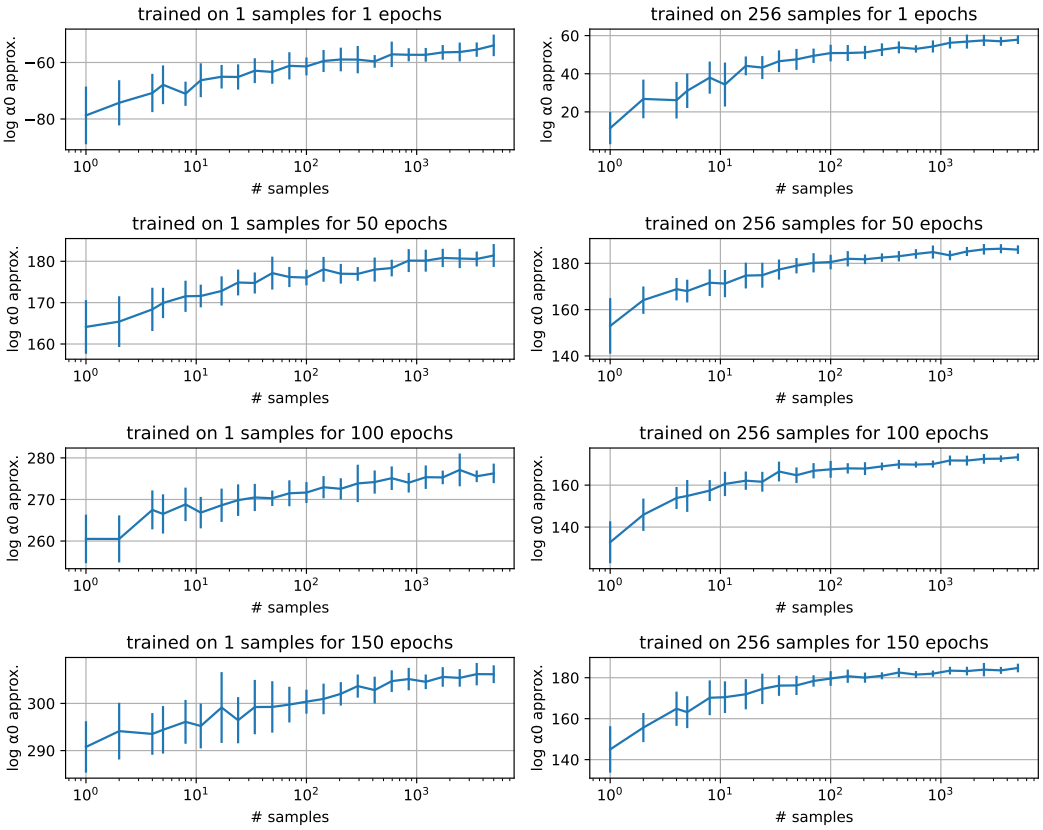


Figure 7: The approximated integral as a function of the number of samples. The left and right columns show the results of models that were trained with 1 and 256 samples, respectively, for the integration approximation. Each row corresponds to a different number of epoch. The y-axis of each graph is the approximated integral value and the x-axis is the number of samples used to approximate the integral post-training. The error bar correspond to 1σ.

standard deviation decreasing when using more samples. This means that our model is consistent and captures the domain well. On the other hand, when using 1 sample, the approximated integral does not saturate and has a different range every epoch. It also shows us that the standard deviations do not decrease even when using more samples. Fig. 7 also shows us that after a few epochs when using a single sample, the approximated integral is very small. This in turn results in a high likelihood which explains the high b/p value for 1sa in Tbl. 2.

E Additional results

E.1 Generator expressiveness and power

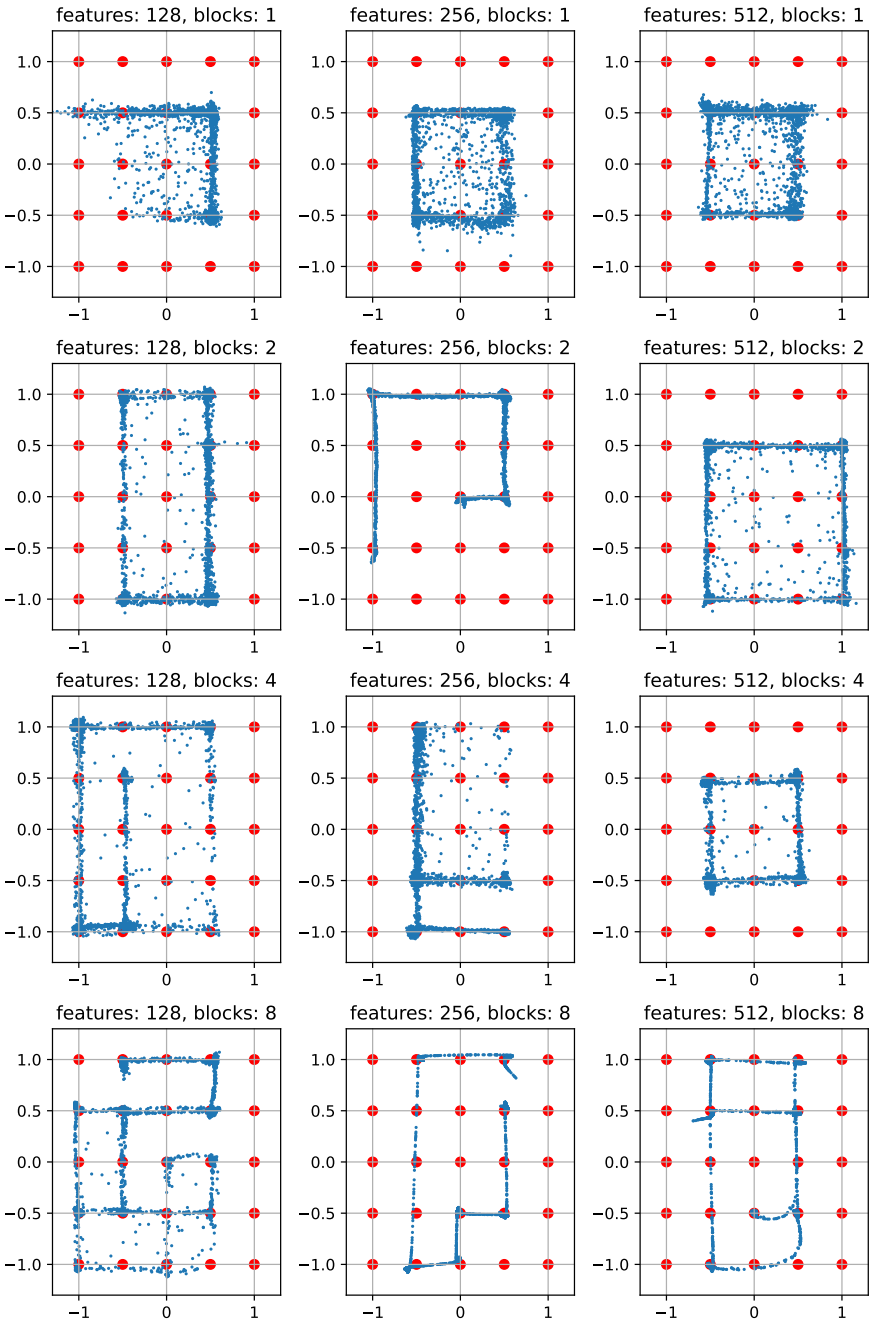


Figure 8: Randomly generated 2D points from generators with different numbers of layers. The generators were trained on the grid of GMMs (Fig. 1g). The red dots represent the true modes and the blue dots are the generated data. Each column corresponds to a different size of latent space (number of features) and each row corresponds to a different number of blocks, as described in Section C.2.

E.2 Generated images sorted by their probability

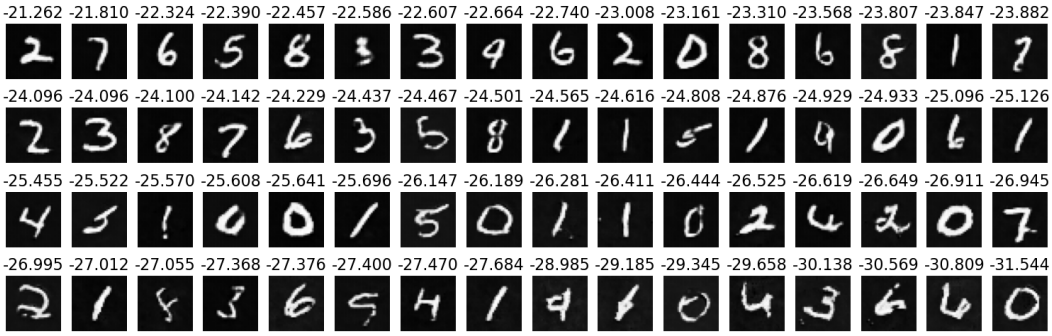


Figure 9: Generated MNIST images, sorted from high probability (top left) to low probability (bottom right). The number above each image is its unnormalized log-likelihood. Note that as the image quality drops, so does the probability.



Figure 10: Generated CelebA images, sorted from high probability (top left) to low probability (bottom right). The number above each image is its unnormalized log-likelihood. Note that as the faces are more deformed, so their probability drops.

E.3 Interpolating the latent space for MNIST

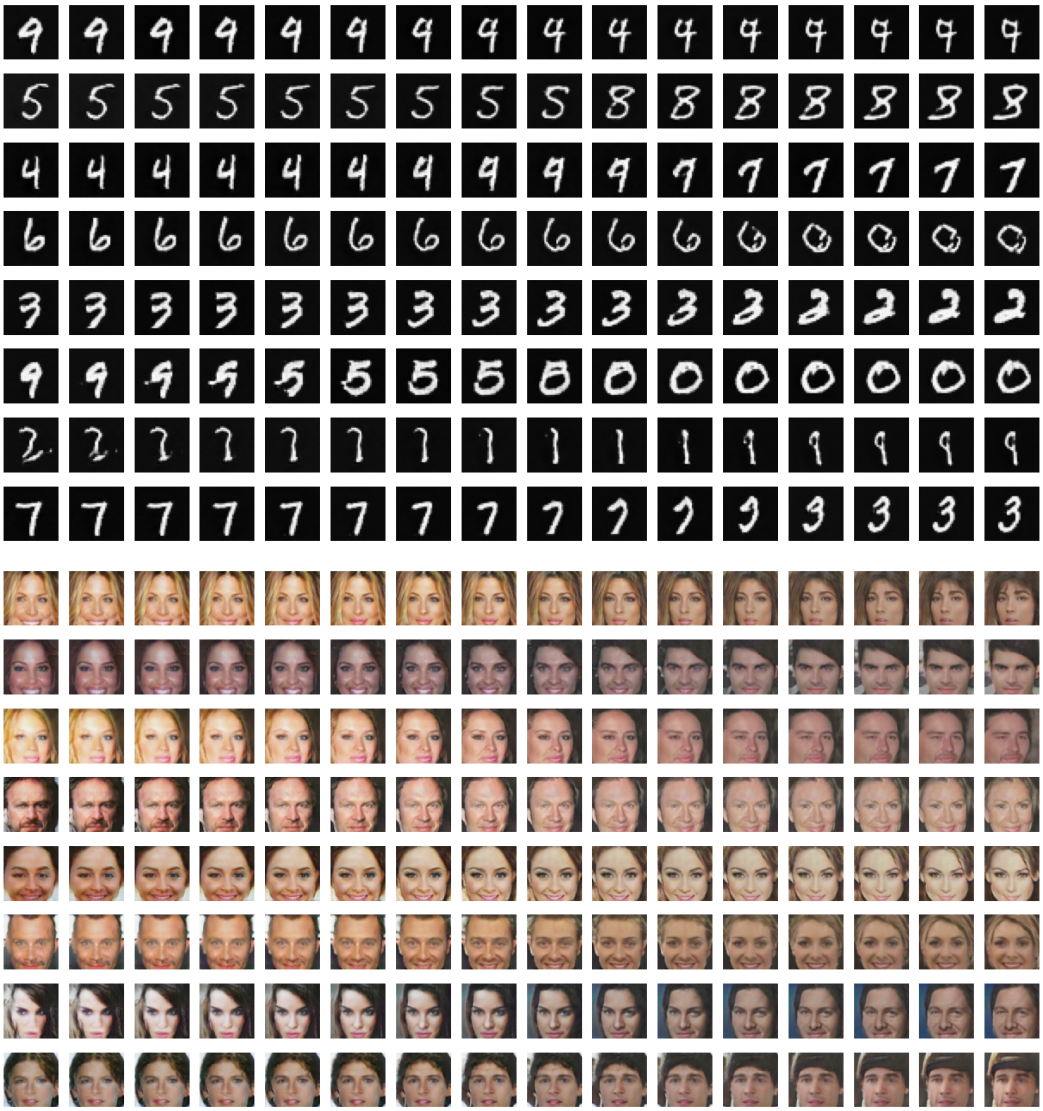


Figure 11: Interpolation over latent space. Each row corresponds to a different interpolation. The leftmost and rightmost columns are images generated by random latent vectors. The images between them are generated by the linear interpolations between the leftmost and rightmost columns.

E.4 Optimizing the latent vector of far away points

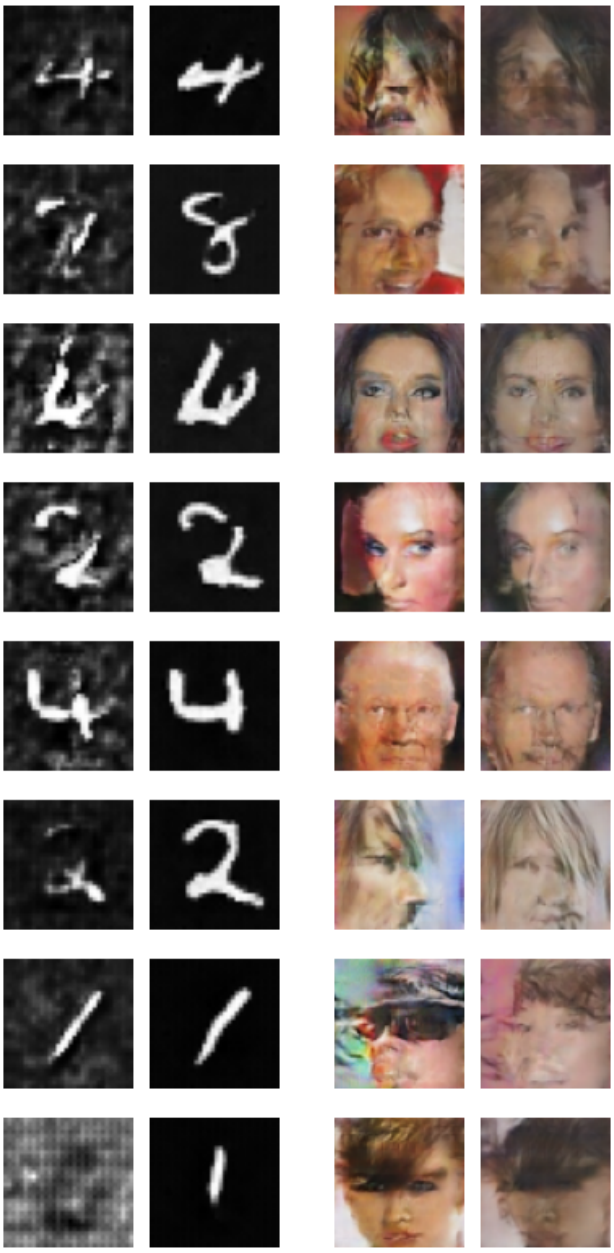


Figure 12: The result of maximizing the discriminator probability by optimizing the latent space. Left column: images generated by the initial latent vectors that are far from the mean (4σ). Left column: the corresponding generated images of the optimized latent vectors. Note that the optimization de-noised some of the background and filled missing holes.